"Depth-Profiling" and Quantitative Characterization of the Size, Composition, Shape, Density, and Morphology of Fine Particles with SPLAT, a Single-Particle Mass Spectrometer

Alla Zelenyuk,*,† Juan Yang,† Chen Song,† Rahul A. Zaveri,† and Dan Imre‡

Pacific Northwest National Laboratory, Richland, Washington 99354, and Imre Consulting, Richland, Washington 99352

Received: September 11, 2007; In Final Form: October 16, 2007

A significant fraction of atmospheric particles are composed of inorganic substances that are mixed or coated with organic compounds. The properties and behavior of these particles depend on the internal composition and arrangement of the specific constituents in each particle. It is important to know which constituent is on the surface and whether it covers the particle surface partially or entirely. We demonstrate here an instrument consisting of an ultrasensitive single-particle mass spectrometer coupled with a differential mobility analyzer to quantitatively measure in real time individual particle composition, size, density, and shape and to determine which substance is on the surface and whether it entirely covers the particle. For this study, we use NaCl particles completely coated with liquid dioctyl phthalate to generate spherical particles, and NaCl particles partially coated with pyrene, a solid poly aromatic hydrocarbon, to produce aspherical particles with pyrene nodules and an exposed NaCl core. We show that the behavior of the mass spectral intensities as a function of laser fluence yields information that can be used to determine the morphological distribution of individual particle constituents.

Introduction

The behavior of fine particles depends on a number of their physical and chemical properties, many of which are strongly coupled. The size, composition, density, shape, morphology, hygroscopicity, activity as cloud condensation nuclei, index of refraction, and other attributes of individual particles all play a role in determining their life cycle and the impact they exert on climate, health, and visibility. To properly include aerosols in environmental models clearly requires knowledge of many of these properties and how they transform in the atmosphere. We have previously described the application of a number of approaches to *simultaneously* measure and quantify several of these attributes for individual particles.[1−5] In this paper, we focus on the extension of these methods to quantitatively measure particle composition while also characterizing the morphological structure of individual particles, that is, which substances are on the surface of the particle and whether they cover the surface partially or entirely.

Answering the question of which substance is at the surface has recently become even more important, since field measurements have shown that organic substances comprise more than 50% of the aerosol mass in many regions around the world. The properties of particles that contain organic substances are subject to changes through heterogeneous reactions with the oxidizing atmosphere, but the rate of reactions between particles and gas-phase molecules such as ozone and OH are expected to be strongly dependent on whether the reacting substances are on the particle surface or inside the particle, shielded from the oxidizing atmosphere. It is therefore important to develop tools and methods that provide us with the capability to determine not only which substances are present but also which ones are on the particle surface.

* Corresponding author. E-mail address: alla.zelenyuk@pnl.gov.
† Pacific Northwest National Laboratory.
‡ Imre Consulting.

The number of studies attempting to directly quantify this property is very limited. Carson et al.[6] reported on a study of crystalline, 3.5 μm NaCl particles that were coated with ammonium nitrate. They showed that by varying the excimer laser power from 0.2 to 1.6 J/cm^2 they were able to "drill" through the ammonium nitrate layer into the particle core. The data show that as the laser power was increased, the mass spectral intensities shifted from being dominated by ammonium nitrate to exhibiting intense NaCl peaks.

Woods et al.[7] reported on an experiment they termed "depth profiling", in which 2.5 μm glycerol particles were coated with relatively thin layers of oleic acid and characterized using a two-laser evaporation/ionization scheme. In that study, an IR pulse generated by either a CO_2 or a parametric oscillator was used to evaporate some of the molecules from the particle, and a UV laser pulse was used to ionize the evaporating plume. They showed that by varying the IR laser power, it was possible to control the relative contribution of the two substances to the mass spectral intensity. At low IR laser power, the mass spectra were dominated by the thin oleic acid coating layer, whereas at higher IR powers, the contribution of the particle core to the mass spectral signature increased significantly. In those experiments, it was also possible to vary the delay between the IR and UV lasers and thereby produce mass spectral signatures that depend on the "time of flight" of the evaporating molecules.

Studies by both Carson et al.[6] and Woods et al.[7] were conducted on rather large particles with relatively wide distributions of sizes. Cai et al.[8] reported results from a mass spectroscopic study of 240 nm polystyrene latex (PSL) particles that were coated with $NaNO_3$, NaCl, and sodium dodecyl sulfate, all of which are sodium containing substances. In this study, the particle mobility and vacuum aerodynamic diameters were measured with very high resolution, which made it possible to calculate the thickness of the coating with 1 nm accuracy. Individual particle mass spectra were generated with an excimer

10.1021/jp077308y CCC: $40.75
Published on Web 01/04/2008

laser that was operated at 2.5 and 5 J/cm^2. These data show that even in these small particles, it is possible to use the dependence of the mass spectral intensity pattern on laser power to identify which of the substances are on the outside of the particle and to simultaneously and quantitatively measure the particle composition, size, density, and shape.

An interesting finding of that study indicates that the mass spectral signature depends not only on which substance is on the outside but also on its morphological distribution on the spherical bead. Not surprisingly, the data clearly show that the PSL core of the particles that are homogeneously coated with $NaNO_3$ are more difficult to detect than when they are coated with NaCl that forms localized cubic nodules on one side of the PSL particle. The morphology of NaCl-coated PSL particles leaves a fraction of the PSL core exposed, making it easier to detect its ions.

In the Cai et al.[8] study, the coating layers were composed of substances that have a very high propensity to form positive ions. To penetrate these coatings required the use of relatively high laser powers, which in turn resulted in extensive fragmentation of the organic polymer and with it a significant loss in mass spectral details. Field data indicate that most atmospheric particles tend to be composed of inorganic substances, such as sulfate, nitrate, or sea salt, that are internally mixed with semivolatile organics. Although the precise particle morphology is not presently known, it is reasonable to assume that in many of these particles, the organic substances can be found on the outside, coating the inorganic core, which in essence is reversed morphology of the one used in the Cai et al. study.[8]

Our goal here is to explore the development of approaches and tools that yield quantitative information on the composition, size, density, shape, and morphology of particles of atmospherically relevant sizes, morphologies, and compositions. Because the mass spectra of most organic molecules tend to be very susceptible to fragmentation at higher laser powers, it is important to test the possibility of generating mass spectra at low laser powers. This approach could preserve sufficient mass spectral details to make identification possible. Here, we will use NaCl as our inorganic core. In addition to serving as a surrogate for sea salt particles, NaCl offers the opportunity to investigate the matrix or charge-transfer effects on the mass spectra of particles that are coated with organics.

In this work, we will explore two coating types: the first is an organic liquid that is expected to encapsulate the NaCl core and form spherical particles, and the second is a solid organic compound that is expected to form aspherical particles composed of a NaCl core with an attached organic nodule. We will investigate the relationship between laser power and the individual particle mass spectral intensity patterns. We will show how the combined measurements of mobility and vacuum aerodynamic diameters offer the possibility to quantitatively determine particle composition, density, dynamic shape factor (DSF), and morphological arrangement.

Experimental Section

Particle Generation and Coatings. NaCl particles are generated by aerosolizing a water solution, using an atomizer (TSI Inc., model 3076). The aerosol flow is then dried by two diffusion dryers (TSI Inc., model 3062) connected in series and classified at 146 nm with a diffential mobility analyzer (DMA, TSI Inc., model 3081). The output from the DMA is passed over a heated source of either dioctyl phthalate (DOP) or pyrene. The temperature of the organics source is varied, while the mobility diameter size distributions of the coated particles are measured by a scanning mobility particle sizer (SMPS, TSI Inc., model 3936). When the desired coating is achieved, the temperature is stabilized, and the coated particles are classified using the second DMA. The system is tested to ensure that no homogeneous nucleation occurs under any of the experimental conditions by eliminating the NaCl seeds and observing the absence of particles.

The data show that mobility diameters of the coated singly and doubly charged NaCl particles are sufficiently different to be easily resolved with the SMPS. As a result, the second DMA can be used to selectively classify either singly or doubly charged particles. For simplicity, most of the data presented here is of singly charged particles, but data of doubly charged particles were also obtained.

Note that in essence, this approach provides the means to experimentally separate particles according to their charges using two DMAs and a coating substance.

Measurements of Vacuum Aerodynamic Diameters and Particle Compositions. The coated particles are sampled by SPLAT, our single-particle mass spectrometer. Since SPLAT has been presented in detail in another publication,[9] we provide here only a few of the relevant points. The vacuum aerodynamic diameters are determined in SPLAT by measuring particle velocities. We have demonstrated that SPLAT has the capability to measure particle aerodynamic diameters with better than 0.5% accuracy. By measuring the mobility and vacuum aerodynamic diameters of individual particles, we obtain particle densities or effective densities also with better than 0.5% accuracy.[2,10] Moreover, we have shown that for aspherical particles of known densities, it is possible to use this information to calculate the particle DSF.[10]

Individual particle mass spectra are generated using an excimer laser operated at 193 nm with pulse length of 15 ns (GAM Lasers Inc., model EX10F). The laser beam is softly focused into a spot that is $\sim$550 μm $\times$ 700 μm in size. The dimension of the laser focal spot represents the measured full width at half maximum (fwhm). Laser power and its pulse to pulse stability are measured using a laser power meter (Molectron, model EM500). Laser power is varied either by reducing the discharge voltage or by attenuating the laser beam.

Mass spectra are obtained using an angular reflectron time-of-flight mass spectrometer (R. M. Jordan, Inc., model D-850) and digitized by an A/D converter (Gage Applied Technologies, Inc., model CompuScope 8500), taking special care to avoid any saturation of either the amplifier or the A/D converter.

Each data point presented in this paper represents the analysis of 500$-$2000 individual particle mass spectra.

Results and Discussions

Spherical Particles. We begin by presenting the results on NaCl particles that are classified by the DMA at 146 nm and coated with DOP. Since the DOP is a liquid, it is expected to coat the NaCl core and form spherical particles. Figure 1 shows the mobility size distribution of uncoated NaCl particles (dashed line) and those of DOP-coated particles (solid line). The former shows a single peak at 146 nm, but in reality, it also contains doubly charged particles with a mobility diameter of 227 nm and a very small number of 301 nm triply charged particles. The mobility size distribution of the coated particles shows two peaks: the more intense peak corresponds to DOP-coated singly charged NaCl particles, now with a mobility diameter of 257 nm, and the less intense peak corresponds to DOP-coated, doubly charged NaCl particles with a mobility diameter of 312 nm.

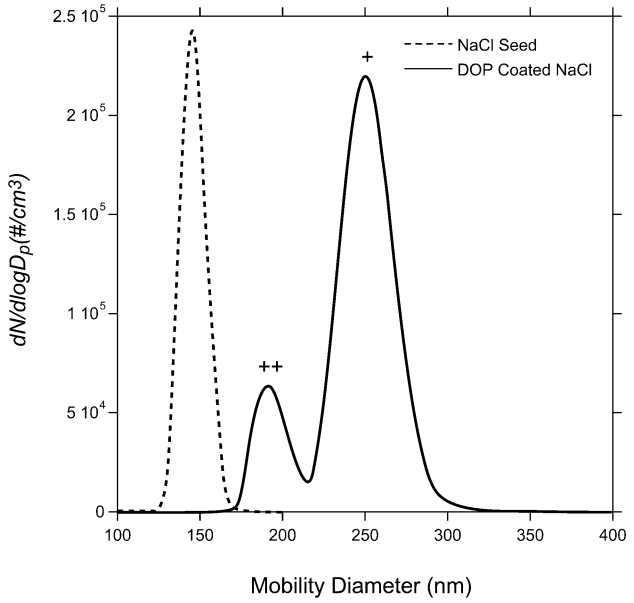

Figure 1. The mobility size distributions of the size-selected NaCl particles that are used as seeds throughout this study (dashed line) and the size distribution of the same particles after they have been coated with DOP. Peaks that correspond to the mobility diameters of singly and doubly charged coated NaCl particles are indicated accordingly.

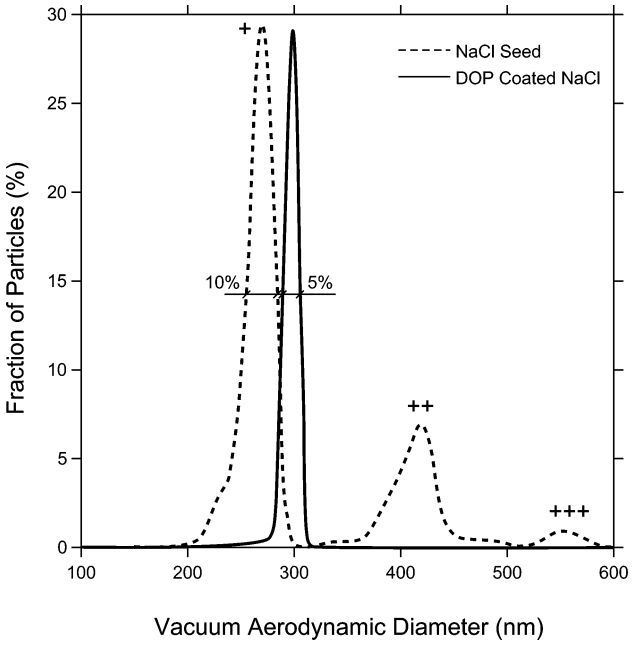

Figure 2. The vacuum aerodynamic size distributions of the NaCl particles that are used as seeds throughout this study (dashed line). Singly, doubly, and triply charged particles are observed and marked accordingly. Note the asymmetric and broad (10% fwhm) line shapes. The solid line shows the vacuum aerodynamic size distributions of coated singly charged NaCl particles with a mobility diameter of 257 nm. The fwhm of this distribution is 5%.

Figure 2 shows the vacuum aerodynamic size distributions of the same particles. The dashed line is that of 146 nm NaCl particles, exhibiting singly, doubly, and triply charged particles. Note that the aerodynamic size distribution exhibits rather asymmetric line shape with a fwhm of 10%. The vacuum aerodynamic size distribution of the coated particles, which is generated by classifying the coated particles with the second DMA to select only singly charged particles, is marked here with the solid line. It shows a single peak with a fwhm of 5%.

The clear difference in the observed line shape of the vacuum aerodynamic size distributions for NaCl and DOP-coated particles is consistent with our previous observations[2,10] that showed that the line shape of the vacuum aerodynamic size distributions of DMA classified particles is dependent on particle shape. In our previous publication, we reported that when aspherical particles such as NaCl are selected by a DMA that is operated with a sheath-to-aerosol flow rate ratio of 10, the fwhm of the vacuum aerodynamic size distributions is 10%. In contrast, the line widths of spherical particles that are classified under the same conditions are 5%.[2,10] These observations provide unquestionable support that these DOP-coated particles are spherical. This last fact also implies that the mobility and vacuum aerodynamic diameters can be used to calculate the true density of the coated NaCl particles according to eq 1,

$$\rho_p = \rho_0 \frac{d_{va}}{d_m} \tag{1}$$

where d_{va} and d_m are particle vacuum aerodynamic and mobility diameters, respectively, and ρ_0 and ρ_p are the unit density and particle density, respectively. Using the measured mobility and vacuum aerodynamic size distributions of the coated singly and doubly charged NaCl particles, we calculate densities of 1.16 and 1.35 g/cm^3, respectively, for these two particle sizes. These values can now be compared to those calculated on the basis of the known NaCl seed size and shape and the size of the coated particles.

To calculate the density of the DOP-coated NaCl particles, we must first calculate the volume fractions of the two components, for which the DSF of the NaCl particles must be taken into account. DSF of the NaCl seed is obtained on the basis of measured mobility and vacuum aerodynamic diameters of the uncoated NaCl particles and known NaCl density using eq 2,[10,11]

$$\frac{d_{va}}{d_m} = \frac{\rho_p}{\rho_0}\frac{1}{\bar{\chi}^2}\frac{C_c(d_{va}\bar{\chi}\rho_0/\rho_p)}{C_c(d_m)} \tag{2}$$

where, $\bar{\chi}$ is the particle DSF, assumed here to be independent of flow regime, and$C_c(d_i)$ are the Cunningham correction factors. The measured d_{va} and d_m of the singly and doubly charged NaCl particles yield DSFs of 1.080 and 1.082 for the NaCl seed particles, respectively. Using the measured mobility diameter and the calculated DSF of 1.08, the volume equivalent diameter, d_{ve}, of the NaCl seed can be calculated from eq 3.

$$d_{ve} = d_m \frac{C_c(d_{ve})}{\bar{\chi} C_c(d_m)} \tag{3}$$

The calculated volume equivalent diameters for the singly and doubly charged NaCl seed particles that are used in this study are found to be 139 and 215 nm, respectively. Combining the measured mobility diameter of the singly charged DOP-coated particles of 257 nm with the calculated volume equivalent diameter of 139 nm of the NaCl seed, we calculate for these particles a DOP coat thickness of 59 nm. Here, we define the coat thickness as the difference between the volume equivalent radii of the NaCl seed and that of the coated particle. The measured mobility diameter of the DOP-coated, doubly charged NaCl particles is 312 nm, which corresponds to a DOP coat thickness of 49 nm.

In this experiment, the two NaCl seed particle sizes are coated under identical conditions, for which, as we show in the

Supporting Information, it is possible to derive eq 4, which relates the changes in the two particle sizes as they are being coated,

$$\lambda(1 - 0.467\alpha)(D_{p1,f} - D_{p1,i}) + 0.1875\alpha({D_{p1,f}}^2 - {D_{p1,i}}^2) - 0.934\alpha\lambda^2 \ln\left(\frac{D_{p1,f} + 2\lambda}{D_{p1,i} + 2\lambda}\right) = \lambda(1 - 0.467\alpha)(D_{p2,f} - D_{p2,i}) + 0.1875\alpha({D_{p2,f}}^2 - {D_{p2,i}}^2) - 0.934\alpha\lambda^2 \ln\left(\frac{D_{p2,f} + 2\lambda}{D_{p2,i} + 2\lambda}\right) \quad (4)$$

where λ is the mean free path in air; α is the mass accommodation coefficient for DOP; $D_{p1,i}$ and $D_{p2,i}$ are the initial seeds' diameters, respectively; and $D_{p1,f}$ and $D_{p2,f}$ are the final diameters of the coated seeds, respectively. It is important to keep in mind that the vast majority of the coating process involves DOP molecules sticking to DOP-coated particles, for which it is reasonable to assume that $\alpha = 1$. Using the measured diameter of the coated singly charged particles and a sticking coefficient of 1, we calculate a final diameter, $D_{p2,f}$ of 313 nm for the doubly charged DOP-coated particles, a result that is in excellent agreement with the measured value of 312 nm. It is worth noting that in this calculation, the calculated final diameter, $D_{p2,f}$, is not very sensitive to the sticking coefficient used.

The volume equivalent diameters of the coated and seed particles are then used to calculate NaCl volume fractions of 0.159 and 0.330 for the singly and doubly charged DOP-coated NaCl particles, respectively. Using the known densities of NaCl (2.165 g/cm^3) and DOP (0.986 g/cm^3), the calculated volume fractions, and the assumption of volume additivity, we calculate densities of 1.17 and 1.37 g/cm^3 for the singly and doubly charged coated particles, respectively. These values are in very good agreement with the measured densities of 1.16 and 1.35 g/cm^3 for the same particles.

The excellent agreement between the calculated and measured densities implies that once the mass spectral data are used to find out the substances that are present in the particle, a quantitative measure of the particle composition can be obtained on the basis of information that is either directly measured here or can be calculated directly from the measurements. This last point leads us to the mass spectral information that is presented in Figure 3.

The left panel of Figure 3 shows a series of average mass spectra obtained by ablating the singly charged DOP-coated NaCl particles with the excimer laser operated at laser fluences that are indicated at the top right corners of each of the corresponding mass spectra. Each of the mass spectra in the figure represents an average of 500−1500 individual particle mass spectra. The first mass spectrum taken at low laser power shows a well-resolved DOP mass spectrum that is very similar to the mass spectrum that is given in the NIST Mass Spectrometry Data Center and was obtained by electron impact ionization of gas-phase DOP at 70 eV. It shows an intense peak at $m/z = 149$, which is characteristic of phthalates. A close inspection of this mass spectrum shows that at this laser power, the presence of NaCl is noted by an extremely weak Na^+ peak. An examination of the mass spectra of the individual particles shows that less than 5% of the individual particle mass spectra exhibit any intensity that corresponds to NaCl.

This last point is important to keep in mind, because in single-particle mass spectrometry, one must consider not only the average mass spectrum but also the properties of the individual particles mass spectra, one of the most important aspects of

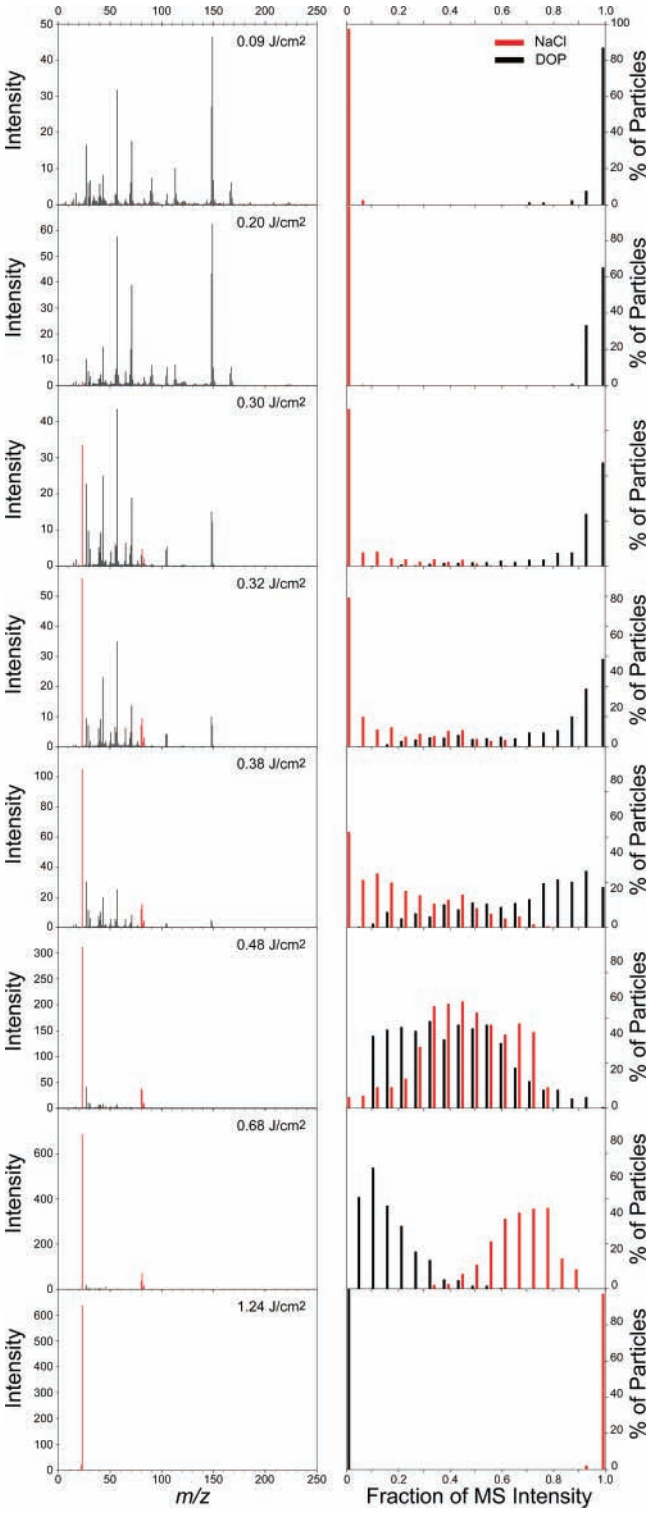

Figure 3. Left panel shows a series of average individual particle mass spectra of NaCl particles with a 59 nm DOP coating obtained at the marked laser fluences. Each spectrum represents an average of over 500 individual particle mass spectra. The right panel shows a statistical analysis of the intensity distributions in the individual particle mass spectra.

which is the particle-to-particle variability in mass spectral intensities. To provide some insight into this aspect of the data, we provide in the right panel of Figure 3 a statistical analysis of the particle-to-particle variability of mass spectral intensities. To generate this plot, the mass spectral intensities are separated into three distinct fractions, with peaks representing DOP, NaCl and the sum of peaks with $m/z = 12$, 24, and 36 to represent

C^+, C_2^+, C_3^+, respectively, which we term a "sootlike" progression. In the present case of a 59-nm-thick DOP coating, the intensity of the sootlike progression remains insignificant for all the laser fluences used in the present study, but it does play a role in thicker coats. The *x* axis in the right panel represents the fraction of the mass spectral intensity, and the *y* axis denotes the fraction of particles that exhibit that distribution.

Given that the particles are constructed to have DOP coating on the outside of the NaCl core, it is extremely encouraging to find a simple trend, in which at the lowest laser fluence, over 90% of the individual particle mass spectral peak intensities are assigned to DOP, and that as the laser fluence is increased, the coating is penetrated and the particle core becomes visible.

An examination of the behavior of the mass spectra as a function of laser fluence reveals a number of trends. Higher laser fluence yields deeper penetration through the DOP coating, as evident from the increase in NaCl mass spectral intensity. Increasing the ablation laser fluence also results in increased fragmentation and loss of the higher DOP *m*/*z* mass spectral peaks intensities. At very high laser fluences, DOP can be fragmented to yield a sootlike mass spectrum dominated by the carbon atom progression, as we mentioned above. The data show that when the NaCl particles in this study were coated with thinner DOP coats of 36 and 59 nm, the sootylike progression is barely observed. In contrast, the mass spectra of the same NaCl particles coated with a 135-nm-thick DOP coat and generated at higher laser fluences contain sootylike carbon atom progression that carries as much as 10% of the total mass spectral intensity. A similar loss in identifiable mass spectral features is seen even for pure NaCl particles, whose mass spectra are reduced to a single Na^+ peak.

The observed increase in NaCl mass spectral peak intensities is a result of the fact that the degree of penetration through the coating increases with laser fluence. The observation that the DOP mass spectral peak intensities decrease and even disappear with increased laser fluence provides a clear illustration of the impact of the matrix and charge-transfer effects. In the present case, we find that when a larger amount of the available Na^+ and Cl^- ions is produced during the ablation process, they successfully compete for charges with the organic fragments, resulting in a drastic decrease in the mass spectral intensities of the organic fraction. This process is possible because it takes place under conditions in which there is a close physical proximity of all the particle constituents within the ablation plume.

The right panel shows that as the laser fluence increases, the fraction of mass spectra that carry a NaCl signature increases. Although 0.48 J/cm^2 is a laser fluence that is sufficient to penetrate the DOP coat of virtually all particles and to produce mass spectral features that indicate the presence of both components, it results in increased fragmentation and significantly diminishes the quality of the DOP mass spectral signature. At even higher laser fluences, all the mass spectra become dominated by NaCl, and at the highest laser fluence, shown in Figure 3 (1.24 J/cm^2), no trace of DOP can be found.

Figure 4 provides a graphic summary of changes in mass spectral intensities as a function of laser fluence for NaCl particles with a 59 nm DOP coating. It shows that when the laser fluence is kept below 0.3 J/cm^2, the average mass spectra are dominated by the DOP coat signature, but that at higher laser fluences, the NaCl signature becomes dominant. At the very high laser fluences, almost no trace of DOP peaks remains. The solid line in this figure and the figures to follow do not represent a theory and are intended only to guide the eye.

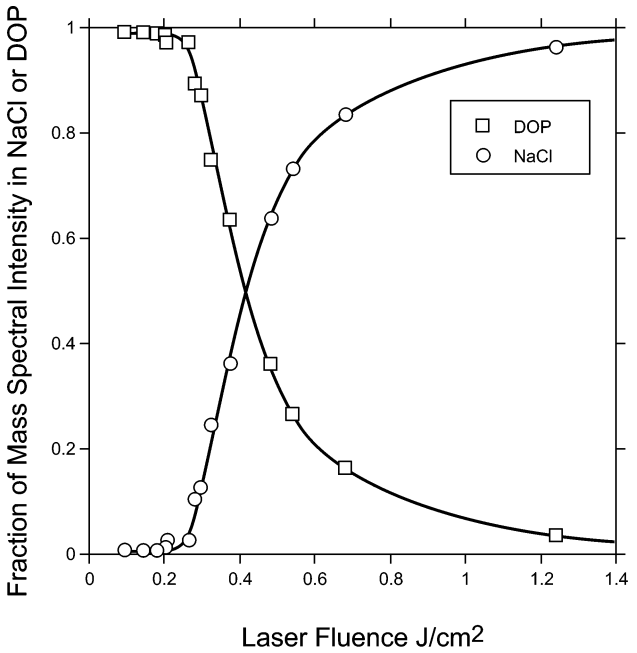

Figure 4. A plot of the fraction of mass spectral peak intensity in the NaCl and DOP peaks as a function of laser fluence for NaCl particles with a 59 nm DOP coat. The solid line is intended to guide the eye.

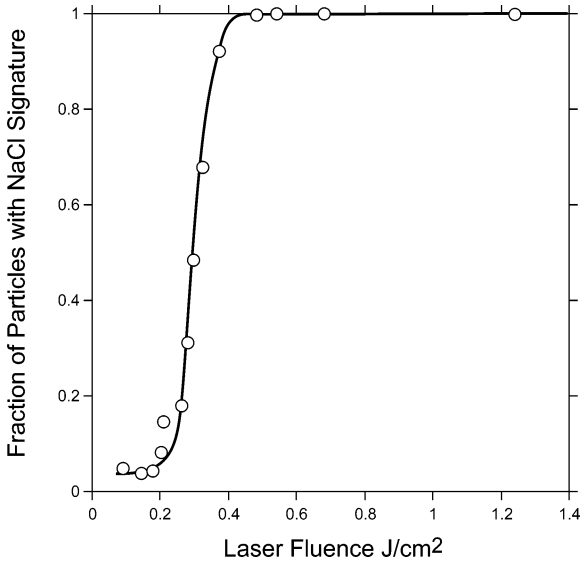

Figure 5. A plot of the fraction of NaCl particles with a 59 nm DOP coat that exhibit NaCl mass spectral signature as a function of laser fluence.

Figure 5 shows a summary of the individual particle mass spectral analysis in a plot of the fraction of particles that carry the NaCl signature as a function of laser fluence. The dependence exhibits a thresholdlike behavior in which at low laser fluence, fewer than 5% of the particles exhibit NaCl mass spectral intensity. An examination of these rare mass spectra reveals that many of them are dominated by NaCl peaks. As the laser fluence increases above 0.3 J/cm^2, the fraction of particles with NaCl signature increases very rapidly, such that when the laser fluence reaches 0.4 J/cm^2, nearly 100% of the particles can be identified as containing NaCl.

If our interpretation of the data is correct, it is reasonable to expect the thickness of the DOP coatings to have a direct impact on the changes in mass spectral intensities as a function of laser fluence. In Figure 6, we present a summary of the data for the same NaCl particles coated with 36-, 59-, and 135-nm-thick

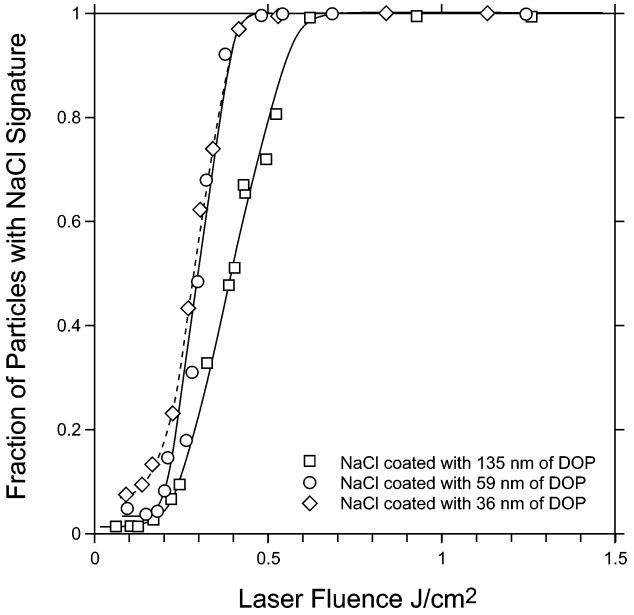

Figure 6. A plot of the fraction of particles that produced NaCl mass spectral signature for NaCl particles coated with 36-, 59-, and 135-nm-thick DOP layers.

TABLE 1: The Measured and Calculated Properties of DOP-Coated NaCl Seeds

d_{ve} NaCl seed (nm)	d_m (nm)	d_{va} (nm)	DOP V_f	DOP W_f	ρ (g/cm^3) meas	ρ (g/cm^3) calcd
139	212	272	0.72	0.535	1.284	1.32
139	257	298	0.84	0.71	1.164	1.17
139	408	427	0.96	0.92	1.046	1.03
215	272	420	0.50	0.32	1.542	1.57
215	312	420	0.67	0.48	1.346	1.37

DOP layers, respectively, in a plot of the probability to detect NaCl ions as a function of laser fluence. The data show that at lower laser fluences, the probability to detect the presence of the NaCl core underneath the 36-nm-thick coat is higher than that for thicker coats. The detection of NaCl seed that is covered with the thinnest DOP coating exhibits a gradual increase as the laser fluence is increased from 0.093 J/cm^2 to slightly above 0.3 J/cm^2, at which point all mass spectra show NaCl intensity. In contrast, the probability to detect NaCl seeds that are covered with a 135-nm-thick coating of DOP is very low at low laser fluences and increases slowly with laser fluence, such that a laser fluence of ~0.6 J/cm^2 is required to reach the point at which all mass spectra contain NaCl peaks. As we noted above, in this case, at higher laser fluences, a presence of "sooty" carbon progression also becomes prominent.

For completeness, we have used the measured mobility and vacuum aerodynamic size distributions to calculate particle densities for the other two coatings that are shown in Figure 6 and have compared those to the calculated densities. These are presented in Table 1. Here, as well, we find perfect agreement between the measured and calculated densities, providing further support for our ability to extract precise, quantitative particle compositions from the measured values.

The changes in mass spectral intensity patterns are consistent with our view of the morphology of these particles. In addition, the data presented in Figures 3, 4, 5, and 6 are all consistent with the picture in which the action of the UV laser is best described by the term "depth profiling", similar to what is described by Woods et al.,[7] except that in the present study, the volume of the particles is 3 orders of magnitude smaller. In this picture, at low laser fluences, the DOP coat shields the NaCl

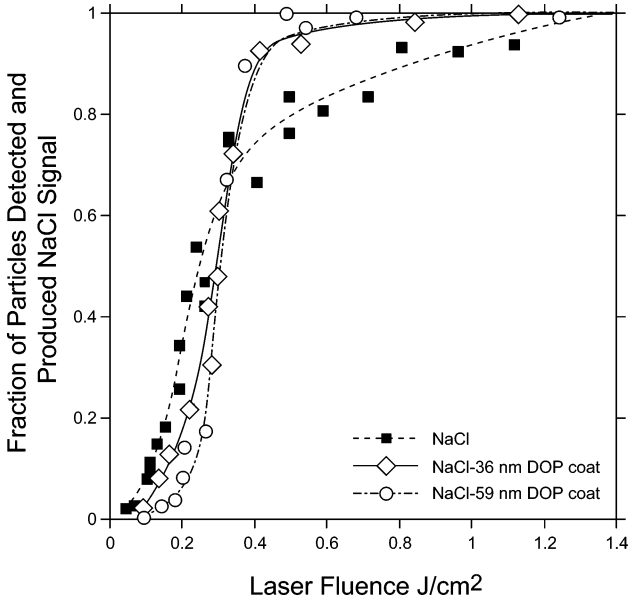

Figure 7. A plot of the fraction of particles that produced NaCl mass spectral signature for pure NaCl particles and NaCl particles with 36- and 59-nm-thick DOP coatings as a function of laser fluence.

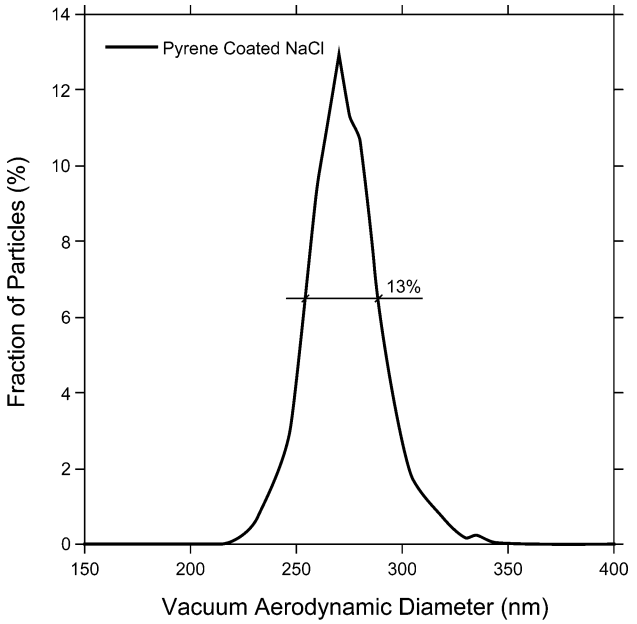

Figure 8. The vacuum aerodynamic size distribution of the pyrene-coated NaCl particles. Note that the fwhm of the d_{va} size distribution is 13%.

core from the laser, making it "invisible", whereas at higher laser fluences, the DOP coat is penetrated to reveal the NaCl core. When Na is evaporated, it competes with the organic fragments for charges, and the mass spectra become dominated by Na^+ ions.

To make sure that the data do not simply reflect the fact that NaCl requires significantly higher temperatures than the semi-volatile DOP to evaporate, we compare in Figure 7 the measurements conducted on DOP-coated particles with those of pure NaCl particles. Figure 7 shows a plot of the probability to form Na-containing ions from pure NaCl particles and that from NaCl particles coated with 36- and 59-nm-thick layers of DOP. Note that the *y* axis in Figure 7 is slightly different from that in Figures 5 and 6. In Figures 5 and 6, we plot the probability of detecting NaCl among all *hits*; in Figure 7, we plot the probability of detecting NaCl among all optically

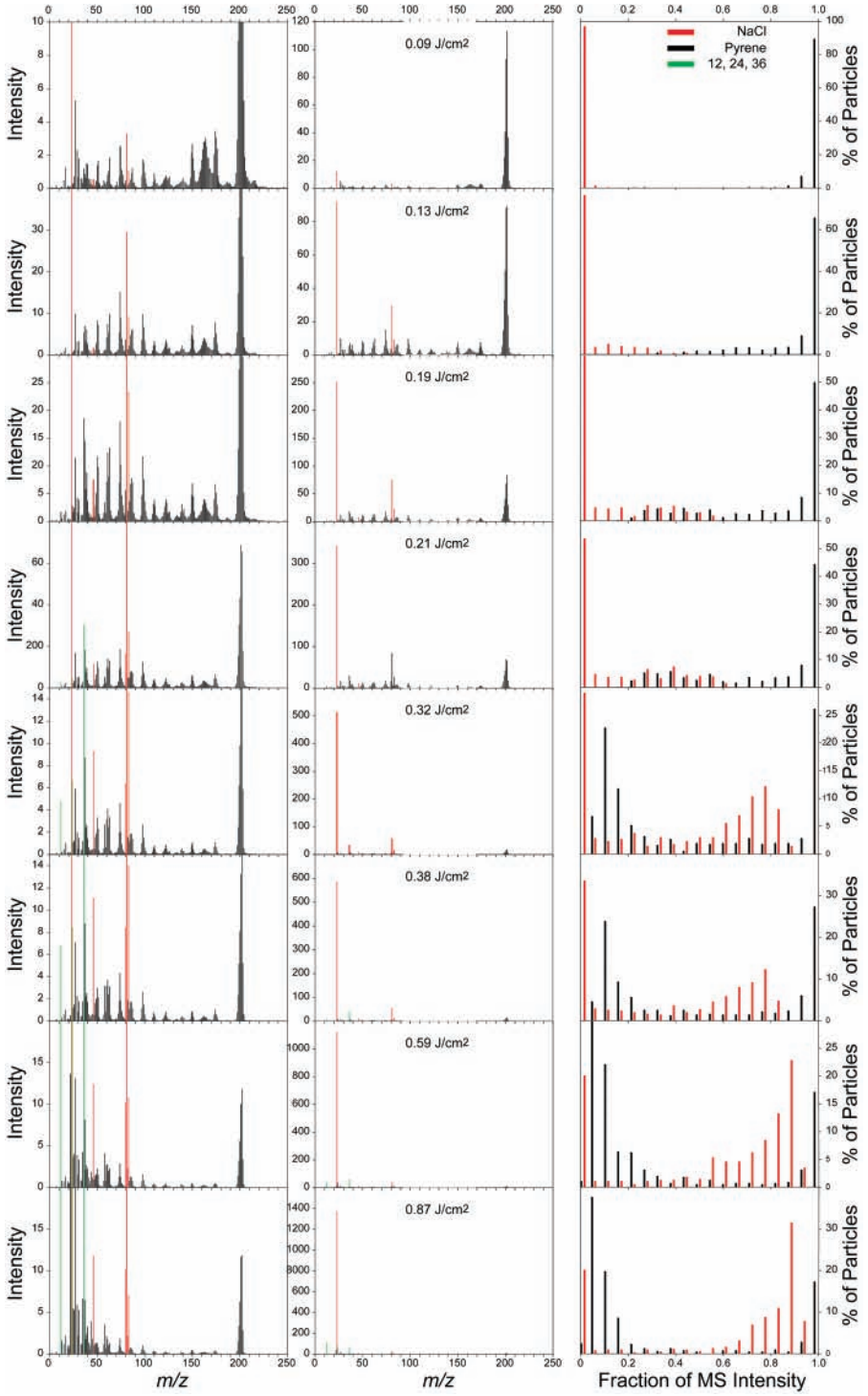

Figure 9. Center panel shows a series of average individual particle mass spectra of NaCl particles with a pyrene coating obtained at the marked laser fluences. Left panel shows the same mass spectra in expanded intensity scales. The right panel shows a statistical analysis of the intensity distributions in the individual particle mass spectra.

detected and properly sized particles, or what may be defined as the NaCl hit rate for DOP-coated and uncoated particles. The pure NaCl data in Figure 7 contain particles with mobility diameters of 150, 234, and 311 nm and exhibit no size dependence. A comparison between the three data sets shows that at lower laser fluence, where the coating is expected to shield the NaCl core, the probability to form ions from pure NaCl is clearly higher than that required to form the same ions from either of the two DOP-coated NaCl seeds.

The data presented in Figure 7 provide support for our previous interpretation that the laser fluence dependence yields information on the morphological distribution of particles' constituents. It is interesting to note that the data suggest that at higher laser fluences, the DOP coating actually increases Na^+ ion production.

Aspherical Particles. The sphericity of the DOP-coated NaCl particles presented us with a relatively simple case, for which it is possible to directly obtain the precise particle composition on the basis of the particles' mass spectra and their mobility and vacuum aerodynamic size distributions. However, many organic compounds found in the atmosphere may exist as solids upon condensation. One may then expect localized nodules of

organics to form on the preexisting particles, such as the NaCl particles used here, while leaving the some parts of the particle surface exposed. As mentioned earlier, the study by Cai et al.[8] showed that the core material can be more easily detected in such partially covered particles than in completely encapsulated particles. We expect to observe similar behavior in the present study, as well.

Here, we use pyrene, a solid poly aromatic hydrocarbon that is commonly found in exhaust pipe emissions, to coat NaCl seed particles. The NaCl seed particles are identical to those used with the DOP coating described earlier. The data presented here are for pyrene-coated NaCl particles with a mobility diameter of 241 nm and a vacuum aerodynamic of 272 nm. Taken together, the mobility and aerodynamic diameters yield an effective density of 1.13 g/cm^3. The vacuum aerodynamic size distribution of these particles is shown in Figure 8. It exhibits a fwhm of 13%, indicating that the coated particles are indeed aspherical, a conclusion that is supported by the fact that the effective density of the coated particles is smaller than the density of either of the two compounds that the particles are composed of (1.271 g/cm^3 for pyrene and 2.165 g/cm^3 for NaCl).

Using the estimated effective density, the measured DSF of the NaCl seeds, their calculated volume equivalent diameter, and the known densities of NaCl and pyrene, the DSF of the pyrene-coated particles is calculated to be 1.155 according to eqs 2 and 3, yielding a volume equivalent diameter of 218.6 nm for the 241 nm pyrene-coated NaCl particles. In other words, the volume fraction of pyrene in these particles is 74.3% and its weight fraction is 63%.

Figure 9 displays the mass spectral information at a number of laser fluences. The center panel shows the average mass spectra obtained at the indicated laser fluences. The left panel shows the same mass spectra plotted at expanded intensity scales, and the right panel provides a statistical analysis of the intensity distributions that are observed in the individual particle mass spectra. Similar to what we have done before with the DOP coating, the mass spectral statistical analysis is divided into three fractions: those representing NaCl, pyrene, and the highly fragmented fraction of pyrene peaks in the form of m/z = 12, 24, and 36. To avoid congestion, the intensity distributions of the latter fraction are not displayed in this plot, but are shown in Figure 10 (discussed below).

Similar to the DOP case, we find that at the lowest laser fluence, the mass spectra are dominated by pyrene, which is indicated by the large intensity of the pyrene parent ion peak. The expanded spectra show clearly that in addition to the parent ion peak, many other pyrene mass spectral peaks are present, but with lower intensities. The most significant difference between the mass spectra of pyrene and DOP-coated particles is the fact that in the pyrene case, NaCl mass spectral peaks carry considerable intensity, even at the very low laser fluences. Moreover, even at these low laser powers, a slight increase in laser power results in a relatively rapid increase in the NaCl peak intensities.

A careful examination of the statistical analysis in the right panel shows that at nearly all laser fluences, two types of mass spectra can be found: ones exhibiting significant Na^+ intensity and others that are dominated by pyrene peaks. What changes with laser fluence is the relative fraction of the two. This pattern is consistent with the expected behavior for a case in which the coating substance does not cover the core surface completely.

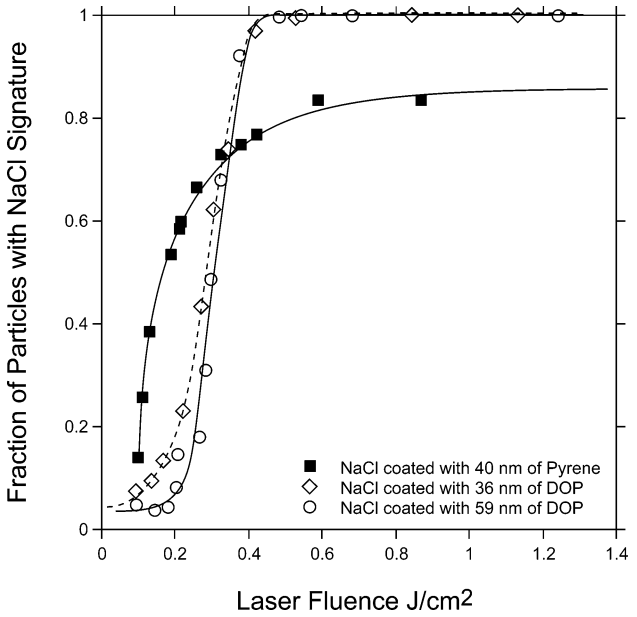

Figure 10. A plot of the fraction of pyrene and DOP-coated NaCl particles that produced NaCl mass spectral signature.

It is clearly also significantly different from the behavior of the NaCl seed particles that are homogenously coated with DOP.

The differences between the two coating types are illustrated in Figure 10. Here, we plot the fraction of particles with detectable NaCl signal as a function of laser fluence for pyrene and DOP-coated particles. Because the pyrene volume and weight fractions fall in between the corresponding values for 212 and 257 nm DOP-coated particles, we included both DOP coatings in the figure. Figure 10 shows that at the lowest laser power, the fraction of mass spectra with a detectable NaCl signal is larger for pyrene-coated particles. Moreover, it increases rapidly with laser fluence and does not exhibit the region in which an increase in laser fluence results in only a minor increase in the NaCl detection probability, as observed for the DOP-coated particles. This again is consistent with a fraction of the NaCl core being at or very near the particle surface, eliminating the need to penetrate a coating.

The differences between the pyrene and DOP coatings are found at the high laser fluences, as well. The data in Figure 10 show that unlike the case of DOP coating, in which at high laser fluences 100% of the mass spectra exhibit the presence NaCl, nearly 20% of the pyrene-coated particles exhibit no NaCl intensity. This observation is consistent with pyrene-coated particles' having regions with localized, very thick pyrene coats. These mass spectra could be representing cases in which the ablation happened to be limited to these regions, and they consequently carry no NaCl signal.

Figure 11 shows an analysis of the behavior of average mass spectral intensities of pyrene-coated particles as a function of laser fluence, subdivided into the three fractions mentioned above. As before, we find that at low laser fluence, the average mass spectra are dominated by the coating substance, and the core intensity increases with laser fluence. Here, the generation of a sootlike progression from pyrene illustrates the tendency of this substance to fragment at high laser fluence. Figure 11 also shows that the NaCl intensity represents only 80% of the overall mass spectral intensity even at the highest laser fluence.

Considering the set of observations on pyrene-coated particles, we can conclude that the data support our assumption that when particles are coated by condensation with solid substances, it is

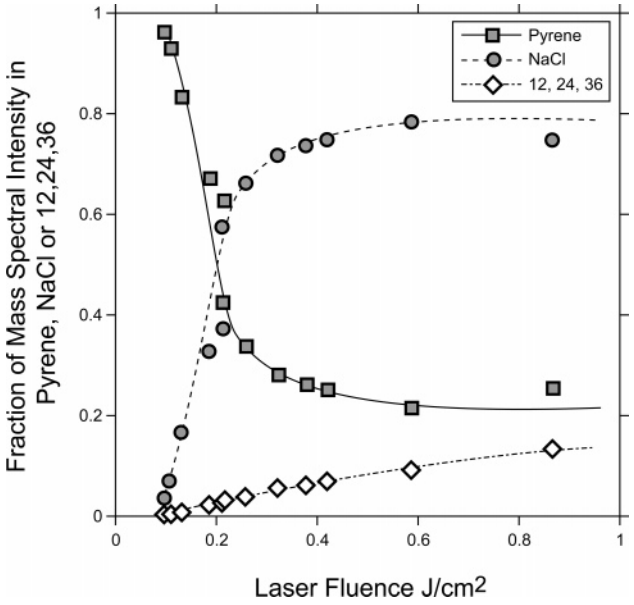

Figure 11. A plot of the fraction of the mass spectral peak intensity in the NaCl, pyrene, and carbon atoms (m/z = 12, 24, 36) peaks as a function of laser fluence for the pyrene-coated NaCl seeds.

likely to form localized nodules with regions of thick coats while leaving a fraction of the particles' core exposed, making it easier to detect the particle core.

Conclusions

We presented the results of a study designed to explore methods to characterize internally mixed particles composed of a mineral substance that is coated with either a liquid or a solid organic. The goal was to test the capability of a single-particle mass spectrometer coupled with a DMA to quantitatively measure the particle size, density, shape, composition, and morphology. We showed that the examination of the mass spectral intensities as a function of laser fluence can be used to identify which of the substances are on the surface and which are inside. The data clearly show that the mass spectra can even be used to find out whether the coating is covering the particle homogenously or if it is localized in some region, leaving some of the particles' cores exposed.

We showed that the mobility and vacuum aerodynamic diameters can be used to obtain a quantitative measure of particle composition, density, and dynamic shape factors. This approach illustrates that a combined system of a high-sensitivity, single-particle mass spectrometer and a DMA can be used as a precise quantitative tool that yields simultaneously many of the key attributes of individual particles.

Acknowledgment. This work was supported by the U.S. Department of Energy Office of Basic Energy Sciences, Chemical Sciences Division. This research was performed in the Environmental Molecular Sciences Laboratory, a national scientific user facility sponsored by the Department of Energy's Office of Biological and Environmental Research at Pacific Northwest National Laboratory (PNNL). Funding for Chen Song and Rahul A. Zaveri was provided by the PNNL Laboratory Directed Research and Development program. PNNL is operated by the U.S. Department of Energy by Battelle Memorial Institute under Contract No. DE-AC06-76RL0 1830.

Supporting Information Available: Additional information as noted in text. This material is available free of charge via the Internet at http://pubs.acs.org.

References and Notes

(1) Buzorius, G.; Zelenyuk, A.; Brechtel, F.; Imre, D. *Geophys. Res. Lett.* **2002**, *29*.

(2) Zelenyuk, A.; Cai, Y.; Chieffo, L.; Imre, D. *Aerosol Sci. Technol.* **2005**, *39*, 972.

(3) Zelenyuk, A.; Imre, D.; Cuadra-Rodriguez, L. A.; Ellison, B. *J. Aerosol Sci.* **2007**, doi: 10.1016/j.jaerosci.2007.06.006.

(4) Zelenyuk, A.; Imre, D.; Han, J.-H.; Oatis, S. Simultaneous Measurement of Size, Composition, Hygroscopicity, and Density of Single Ambient Particles; Eos Trans. AGU, 2003.

(5) Zelenyuk, A.; Imre, D.; Han, J.-H.; Oatis, S. *Anal. Chem.* **2007**, Submitted.

(6) Carson, P. G.; Johnston, M. V.; Wexler, A. S. *Aerosol Sci. Technol.* **1997**, *26*, 291.

(7) Woods, E.; Smith, G. D.; Miller, R. E.; Baer, T. *Anal. Chem.* **2002**, *74*, 1642.

(8) Cai, Y.; Zelenyuk, A.; Imre, D. *Aerosol Sci. Technol.* **2006**, *40*, 1111.

(9) Zelenyuk, A.; Imre, D. *Aerosol Sci. Technol.* **2005**, *39*, 554.

(10) Zelenyuk, A.; Cai, Y.; Imre, D. *Aerosol Sci. Technol.* **2006**, *40*, 197.

(11) DeCarlo, P. F.; Slowik, J. G.; Worsnop, D. R.; Davidovits, P.; Jimenez, J. L. *Aerosol Sci. Technol.* **2004**, *38*, 1185.

(12) Fuchs, N. A.; Sutugin, A. G. High-Dispersed Aerosols. In *Topics in Current Aerosol Research*; Hidy, G. M., Brock, J. R., Eds.; Pergamon: New York, 1971; Part 2; pp 1.